Acoustic emission during the tensile deformation of Incoloy 901 superalloy

DAINING FANG*, AVRAHAM BERKOVITS†
Faculty of Aerospace Engineering, Technion–Israel Institute of Technology, Haifa 32000, Israel

Observations have been made on the acoustic emission (AE) response related to the deformation–damage mechanisms during tensile tests of a common engine material, Incoloy 901 superalloy. Results show that dislocation motion, twinning and inclusion fracture cooperated to generate acoustic emission during tensile deformation of Incoloy 901. Based on AE recorded results and microstructural examination, a dislocation–saturation model was developed to describe AE activity during elastic and plastic deformation, and to distinguish between the AE response in the yield region and in the work-hardening region. Furthermore, the effects of strain rate and loading methods on AE outputs were examined. The dependence of acoustic emission on dislocation motion and saturation, deformation twinning, and decohesion and fracture of inclusions and secondary particles are discussed.

1. Introduction

Acoustic emission (AE) can be detected in materials during elastic–plastic deformation due to applied stress. Many mechanisms have been confirmed as AE sources, including slip (dislocation motion) [1–5], twinning [6–9] and the decohesion and/or fracture of inclusions and second phase particles [10–13]. Identifying the actual sources of the acoustic emission is difficult since the data may consist of emissions from several sources which may be operating either independently or in cooperation. References in several reviews [2, 4, 7] show that numerous investigations have been carried out to characterize acoustic emission and reveal the relation between deformation mechanisms and AE activity. Nevertheless, few models have been developed to describe the relation of AE activity and increasing strain during the elastic–plastic deformation.

There are no fundamental works which examine the AE activity characteristics of complex nickel-base superalloys. This kind of superalloy is widely used for aerospace components, such as engine disc parts. The investigation of damage in nickel superalloys under both static and cyclic loading has been of increasing concern over recent decades. The present paper is focused on investigating the relation of acoustic emission activity to tensile strain and AE source characteristics associated with the microstructural variation of Incoloy 901 during elastic–plastic tensile deformation at room temperature. In this investigation, AE activity in the pre-yield, yield and work-hardening regions was studied, and the effects of loading methods and loading rates on AE activity and micromechanism were examined.

2. Experimental procedure
2.1. Material and specimen

The work was carried out on nickel-base Incoloy 901 superalloy taken from a new engine disc conventionally cast and forged. The composition of the material has been given elsewhere [14–15]. A typical optical micrograph of the virgin material is shown in Fig. 1. The material is a precipitation hardening alloy with a stable austenitic matrix and γ' (Ni_3Ti) phase precipitates. The grain size ranges from 100 to 200 μm. Brittle inclusions or particles are dispersed in the matrix and along the grain boundaries. The material contains growth twins [18–19], formed during crystal growth on solidification and recrystallization during casting and forging. The flat test specimen was designed according to ASTM standard E466 [20]. Specimens were prepared from radial plates cut from the turbin disc, such that the minimum section of all specimens lay at a single radial distance from the hub of the disc. Thus uniformity of composition, microstructural and mechanical properties was ensured in the test section of all specimens.

2.2. AE tensile testing procedure

All monotonic tensile tests were performed at room temperature on a MTS electrohydraulic test machine. Load was applied at either constant
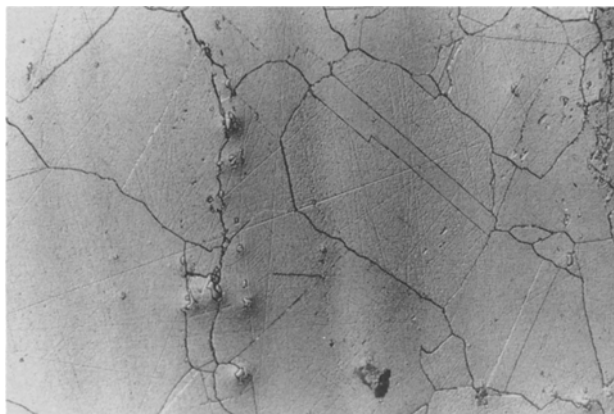
Figure 1 Optical micrograph of virgin Incoloy 901 superalloy (50 μm).

data and smoothed), as well as the integral of the AE ringdown counts.

crosshead speed (stroke-controlled) or constant strain rate (strain-controlled) in order to examine differences in AE activity and mechanisms due to the loading methods.

Acoustic emission was detected by a Babcock and Wilcox AET 5500 computerized monitoring system with a total system gain of 94 dB and a floating signal threshold at a level of 15 dB. The preamplifiers had 60 dB gain with a 250–500 kHz bandpass filter. Three 300 kHz piezoelectric sensors with 2 dB sensitivity were clamped on the specimens to constitute a three-channel linear location guard array. The rejection of high extraneous background signals from hydraulic, electrical and mechanical noise was of paramount importance. Various AE test techniques developed and reported previously [14–17], were used in combination during the tests.

3. Results

Typical AE counting output and stress–strain results are presented in Fig. 2. Superimposed on the stress–strain curve are the AE ringdown count rate (raw

3.1. Examination of the microstructure of deformed samples

Figs 3 and 4 are optical micrographs of two specimens tested at constant crosshead speed of 0.4 mm min^{-1} and 2.5 mm min^{-1}, respectively. Various typical microstructural characteristics are evident in the micrographs, such as slip bands, twinning, fracture of inclusions and secondary phase γ' particles and microvoid coalescence, all of which contribute to AE output. The slip plane is $\{1\,1\,1\}$, on which the shape of etch pits is typically triangular. The slip was dispersed around some of the grains but not in twins. Not only were straight rows of etch pits representing dislocations to be found, but etch pits were also dispersed along the slip bands and grain boundaries, revealing that there were a large number of dislocation pile-ups in the grain boundaries. Coarse slip band formation shows that there were several slip systems in the $\langle 1\,1\,0 \rangle$ direction. Fewer slip bands corresponds to more twinning since twin layers hinder propagation of slip.

The twin plane was also $\{1\,1\,1\}$ and the presence of etch pits along the twin lines in Figs 3 and 4 illustrates that there was a large amount of dislocation pile-up along the twin lines. From the micrographs it can be seen that there were two kinds of twin, one which traversed the entire grain, called a complete twin, and an incomplete twin, one end of which was attached at the grain boundary while the other end was located within the grain. The statistical results for twins given in Table I highlight that not only did growth or nonlinear twins exist before deformation, but also nucleation and deformation of twinning occurred during the tensile deformation. Considerable fracture and decohesion of inclusions and secondary phase (Ni_3Ti) particles occurred both inside grains as well as along the grain boundaries. The mechanisms of these microstructural characteristics
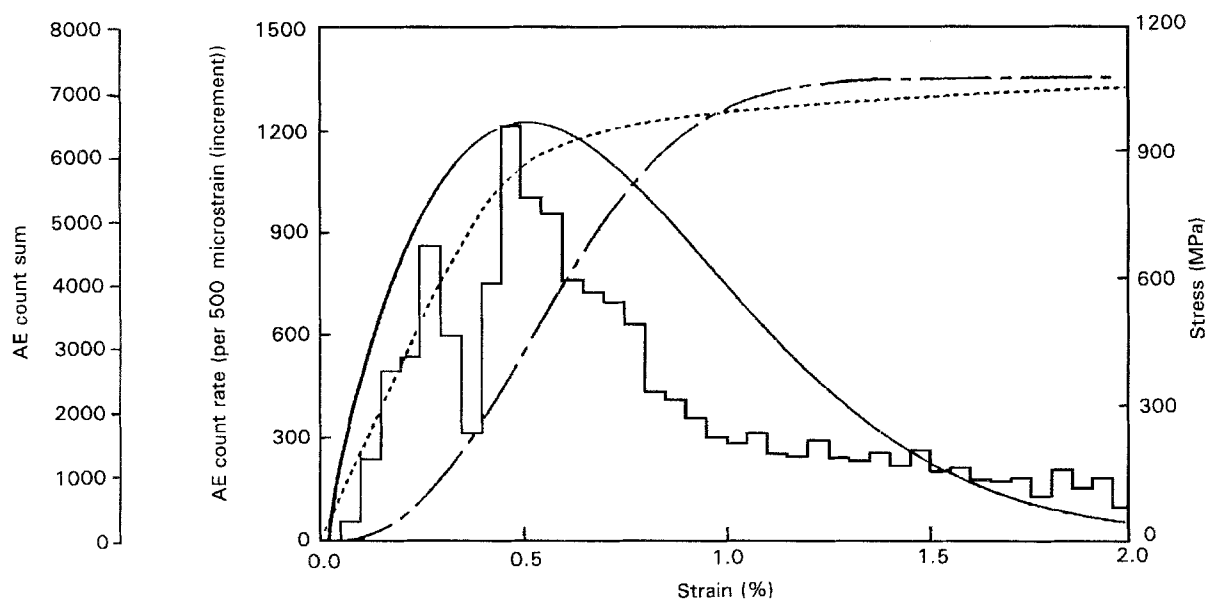

Figure 2 Tensile stress–strain curve and AE output ...., stress versus strain; ———, count rate; ————, count sum.
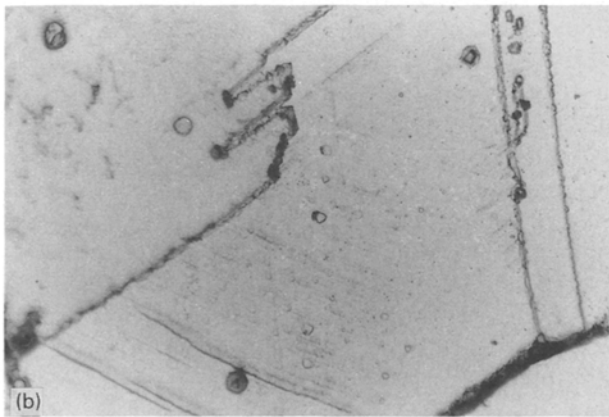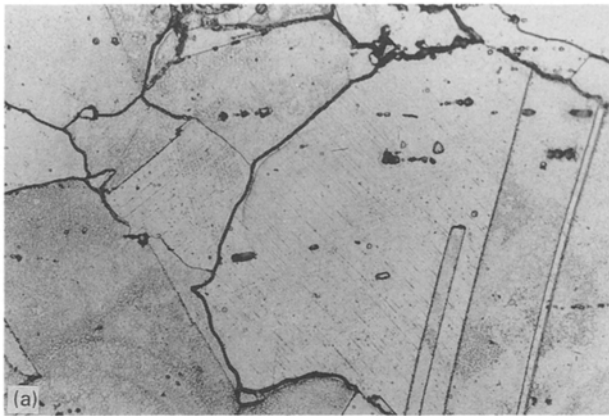
Figure 3 Optical micrographs of Incoloy 901 fracture sample tested at 0.4 mm min^{-1} crosshead speed. (a) 50 μm, and (b) 1 μm.
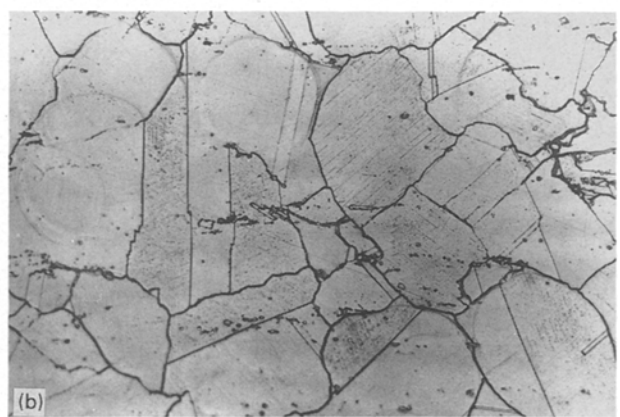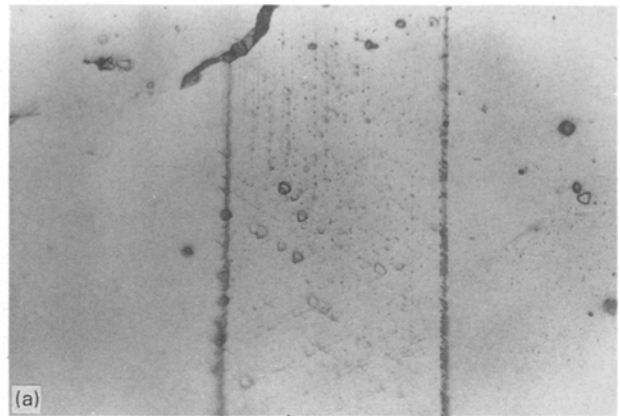
Figure 4 Optical micrographs of Incoloy 901 fracture sample tested at 2.5 mm min^{-1} crosshead speed. (a) 1 μm, and (b) 100 μm.

associated with AE origin and activity will be discussed later.

3.2. Acoustic emission due to strain
An attempt was made to explain the shape of the AE curves and the amount of acoustic emission observed as a function of strain. The rate of ringdown count per strain ($d\eta/d\varepsilon$) and cumulative total ringdown counts (η) against strain are recorded in Figs 5 and 6. According to the energy analysis [1–2, 14], one can consider yielding as the result of random dislocation motion and saturation. The rate of ringdown counts per strain $d\eta/d\varepsilon$ in the yield region could be described by the

Weibull function

$$\frac{d\eta}{d\varepsilon} = g \times \exp\left[-\left(\frac{\varepsilon - \varepsilon_0}{a_2}\right)^{a_1}\right] \bigg/ (\varepsilon - \varepsilon_0)^{(1-a_1)} \quad (1)$$

where g is the total number of ringdown counts, ε_0 is the strain necessary to initiate AE activity, a_1 and a_2 are scale and shape constants respectively. This means that the density of sources capable of producing detectable avalanches and pockets of moving dislocations had a Weibull distribution. The smoothed AE curve in Fig. 2 was achieved by use of the Weibull function. However, Figs 5 and 6 show that the actual AE output continued during the work-hardening region due to the sources from fracture of inclusions or γ' particles,

TABLE I Distribution of twins in Incoloy 901

Specimen	Location	Crosshead speed (mm min^{-1})	Complete twins per mm^2		Incomplete twins per mm^2		Width of twins (μm per mm^2)	
			E_n	S_n	E_n	S_n	E_w	S_w
0304	Grip-section	0 (new)	9.74	2.56	1.88	1.09	26.86	2.39
ST0414	Grip-section	0.4	12.76	3.57	2.42	1.16	26.86	2.33
	Test-section		17.12	2.39	3.36	1.70	37.6	2.87
ST0504	Test-section	2.5	20.68	3.04	4.23	2.23	44.99	3.40

E_n, average density. S_n, standard deviation of twin density. E_w, average twin width per unit area. S_w, standard deviation of twin width per unit area.
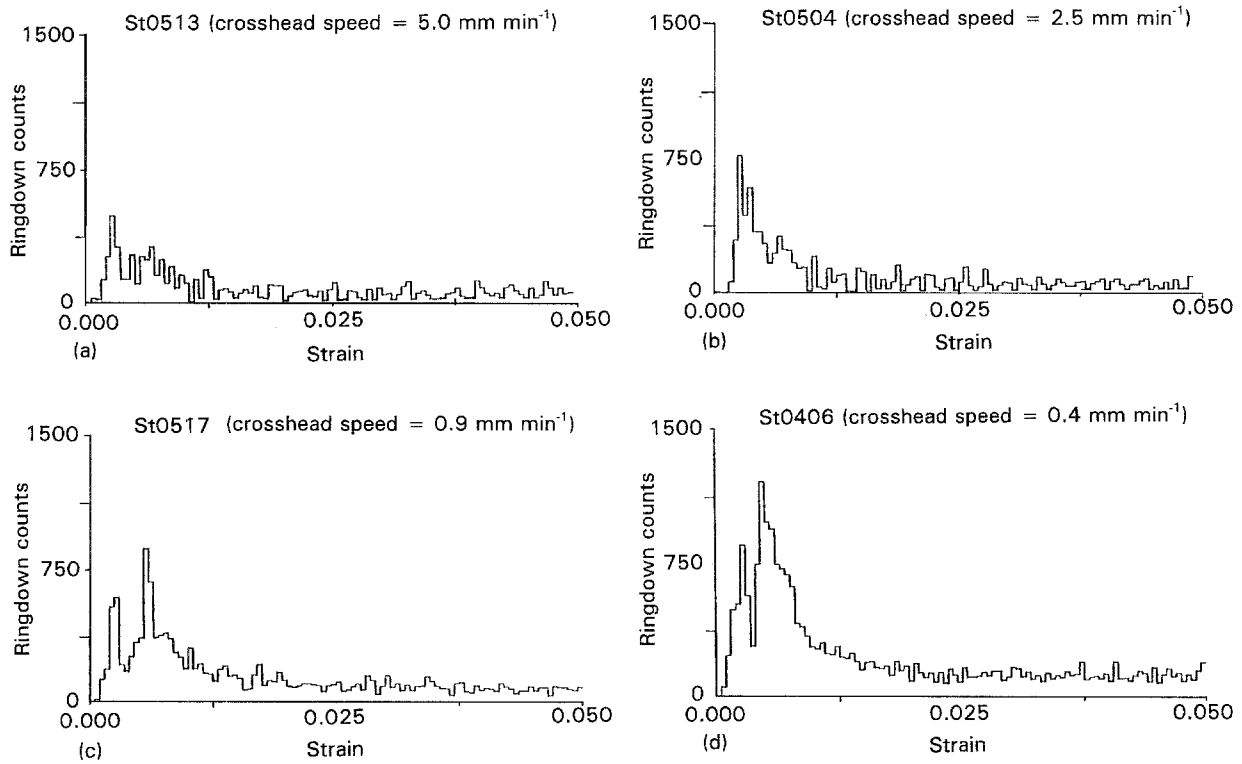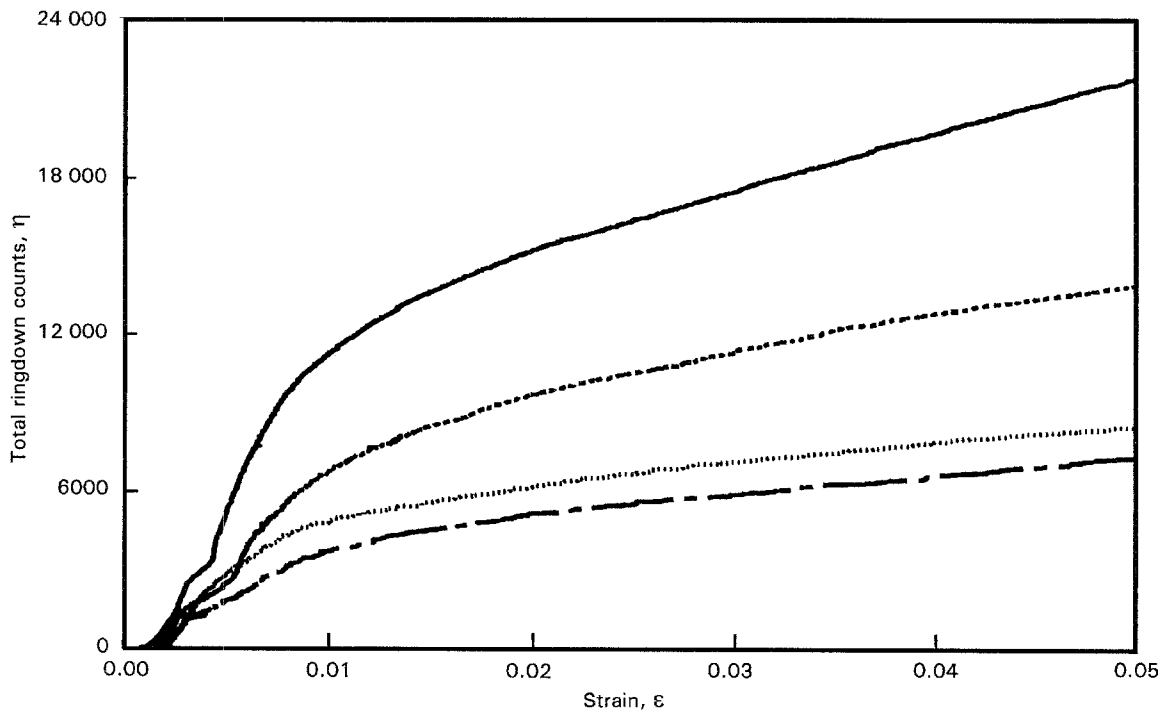
Figure 5 Strain-dependence of AE counts.

Figure 6 Strain dependence of total ringdown counts, ———, ST0406 $(0.4 \text{ mm min}^{-1})$; ——, ST0517 $(0.9 \text{ mm min}^{-1})$; ...., ST0504 $(2.5 \text{ mm min}^{-1})$; —·—· , ST0513 $(5.0 \text{ mm min}^{-1})$.

twinning and occasional breakaway of dislocation pile-ups, so that Equation 1 could not cover the whole AE activity process during the tensile deformation. Therefore, a more general model was developed to describe the relation between AE activity and increasing strain, in Fig. 7. This model distinguishes between AE output in the yield region and in the work-hardening region.

Upon examination of the experimental results, it was found that a_1 in Equation 1 is very close to 2 for

Incoloy 901. Then in the yield region, the Weibull function can be expressed more conveniently as

$$\eta_y(\varepsilon) = \eta_s \times \left\{ 1 - \exp\left[-\left(\frac{(\varepsilon - \varepsilon_0)^2}{2d^2} \right) \right] \right\} \quad (2)$$

$$\frac{d\eta_y}{d\varepsilon} = \frac{\eta_s}{d^2} \times (\varepsilon - \varepsilon_0) \times \exp\left[-\left(\frac{(\varepsilon - \varepsilon_0)^2}{2d^2} \right) \right] \quad (3)$$
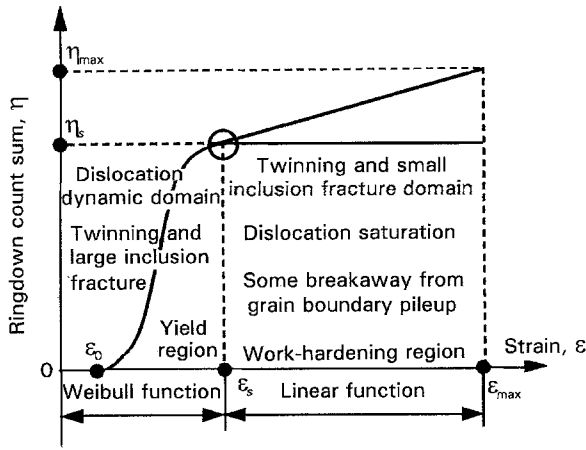
3555

Figure 7 Schematic of the model of AE-count sum dependence on strain in constant crosshead-rate tension.

where η_y is the cumulative total count in the yield region, and η_s is the count number corresponding to the dislocation saturation level (see Fig. 7). The limiting conditions based on dislocation motion saturation in the yield region can be listed as

$$\eta_y = 0 \quad \text{if } \varepsilon < \varepsilon_0 \tag{4}$$

$$\frac{d\eta_y}{d\varepsilon} > 0 \quad \text{if } \varepsilon_0 \leq \varepsilon \tag{5}$$

$$\frac{d\eta_y}{d\varepsilon} = \text{constant} \quad \text{if } \varepsilon \geq \varepsilon_s \tag{6}$$

where ε_s is the strain corresponding to the dislocation saturation moment

$$\varepsilon_s = \beta \times \varepsilon_y \tag{7}$$

where ε_y is the yield strain and β is an empirical constant obtained from the strength tests. For Incoloy 901 ε_s is about 0.012–0.015. Under the test conditions of 94 dB system gain and 15 dB threshold, ε_0 obtained from AE signatures of Incoloy 901 was on the order of 0.003. Using the critical condition of the saturation process, in Equation 6 one may evaluate constant.

$$d = d(\varepsilon_s, \varepsilon_0). \tag{8}$$

The total counts curve in Figs 6 and 7 can now be expressed as

$$\eta_t = \begin{cases} \eta_t & (\varepsilon_0 \leq \varepsilon < \varepsilon_s) \\ \eta_w & (\varepsilon \geq \varepsilon_s) \end{cases} \tag{9}$$

where η_t is the cumulative total counts throughout the whole deformation, and η_w is the total counts in the work-hardening region. From Figs 5 and 6 it is seen that $d\eta_w/d\varepsilon$ is almost constant, so that η_w is a linear function of strain (see Fig. 7)

$$\eta_w = K_1 \times \varepsilon + K_2 \quad \text{if } \varepsilon \geq \varepsilon_s \tag{10}$$

Equation 10 must be compatible with the boundary conditions of the work-hardening region. That is, when $\varepsilon = \varepsilon_s, \eta_w = \eta_y$ and when $\varepsilon = \varepsilon_f, \eta_w = \eta_f$, so

that

$$\begin{cases} k_1 = \eta_f - \varepsilon_f \left(\dfrac{\eta_f - \eta_s}{\varepsilon_f - \varepsilon_s} \right) \\ k_2 = \dfrac{\eta_f - \eta_s}{\varepsilon_f - \varepsilon_s} \end{cases} \tag{11}$$

Based on the experimental results and the relationship between cumulative counts η_t and strain (Equations 2, 9 and 10), the AE sources during Incoloy 901 tensile deformation corresponded to three stages:

(i) *Pre-yield region.* (a) Twinning; (b) fracture and decohesion of larger inclusions and γ' particles; (c) small amount of dislocation break-away from pins, grain-boundary activity, with relatively small pockets of moving dislocation.

(ii) *Yield region.* (a) Significant dislocation motion, dislocation avalanching, significant multiplication reaching a maximum, increased velocity and slip propagation, and coarse slip-band formation; (b) twinning; (c) fracture and decohesion of inclusions and γ' particles.

(iii) *Work-hardening region.* Dislocation dynamics approach saturation, most of the AE sources being associated with: (a) fracture and decohesion of inclusions and γ' particles; (b) twinning; (c) small amount of break-away of dislocation pile-ups on interfaces such as the grain boundaries and nonlinear thermal twin lines.

For most materials, the AE activity in the pre-yield stage is relatively weak [1–7] so that it can be incorporated into that of the yield stage. Thus, AE origin and activity was described in two regions (Fig. 7): the yield region ($\varepsilon_0 \leq \varepsilon < \varepsilon_s$) with the dislocation dynamics domain described by Equation 2; and the work-hardening region ($\varepsilon \geq \varepsilon_s$), with inclusion fracture and twinning domain if such occur in the materials.

3.3. Effect of strain rate on AE

There is consensus concerning the dependence of acoustic emission on strain rate than on other experimental parameters [1–2,4,21–23]. In general, V_{rms}, the square of the voltage of the AE signal, is observed to be proportional to strain rate, so that

$$V_{rms} \propto A\dot{\varepsilon}^{1/2} \tag{12}$$

It has been shown that the count rate $d\eta/dt$ is given by

$$\dot{\eta} = \frac{d\eta}{dt} = f \times \exp\left[-\frac{V_{th}^2}{BV_{rms}^2} \right] \tag{13}$$

where f is the apparent frequency of the signal, V_{th} is the threshold voltage and $B \approx 2$. The dependence of count rate on strain rate can be seen by substituting Equation 12 into Equation 13. This was observed in the experimental results shown in Fig. 8. Although larger $\dot{\varepsilon}$ led to larger count rate $\dot{\eta}$, it also resulted in small $d\eta/d\varepsilon$, as seen in Figs 5 and 6. The fact that the influence of strain rate on $\dot{\eta}$ was positive while it was negative on η and $d\eta/d\varepsilon$ shows that the AE response
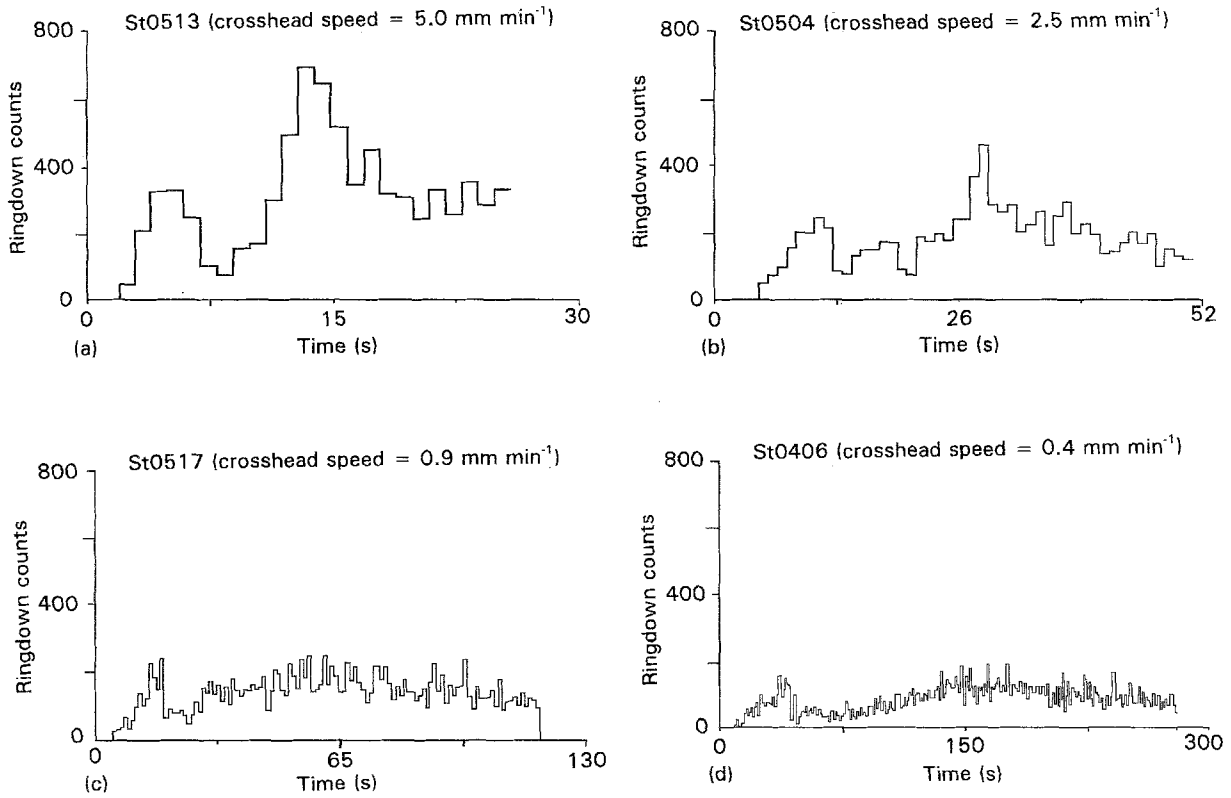
3556

Figure 8 Time-dependence of AE counts.

during monotonic deformation is a time-dependent process. Noting the statistical results shown in Table I, it is clear that the mechanism responsible for producing acoustic emission is altered by a change in strain rate. The faster the crosshead speed, the more twins and fewer slip bands occur. Therefore, it may be assumed that the continuous-type signals from slip or dislocation motion contribute more AE events and counts than other sources such as twinning and inclusion fracture. In addition, at short deformation time, the burst signals are more likely to overlap one another, which also leads to an apparent reduction of cumulative counts.

3.4. Effects of loading method on AE

The above analysis was based on experimental results obtained from tensile deformation at constant, stroke-controlled crosshead speed. Results of tensile deformation under constant, strain-controlled strain rate are shown in Figs 9 and 10. Both count rates and total count sums differed from results shown in Figs 5, 6 and 8. $d\eta/d\varepsilon$ and $d\eta/dt$ were almost constant with increasing plastic strain except for a small peak near yield (see Fig. 9), and the count sum was consequently almost linearly increasing with increasing strain. The effect of the deformation rate on AE output seen in stroke-controlled tests was also observed in strain-controlled tests, presented in Fig. 10.

The difference between experimental results obtained from the two loading methods used implied that plastic strain rate $\dot{\varepsilon}_p$ controls the deformation mechanism and AE output. A well known relationship between $\dot{\varepsilon}_p$ and dislocation parameters [18–19] can be

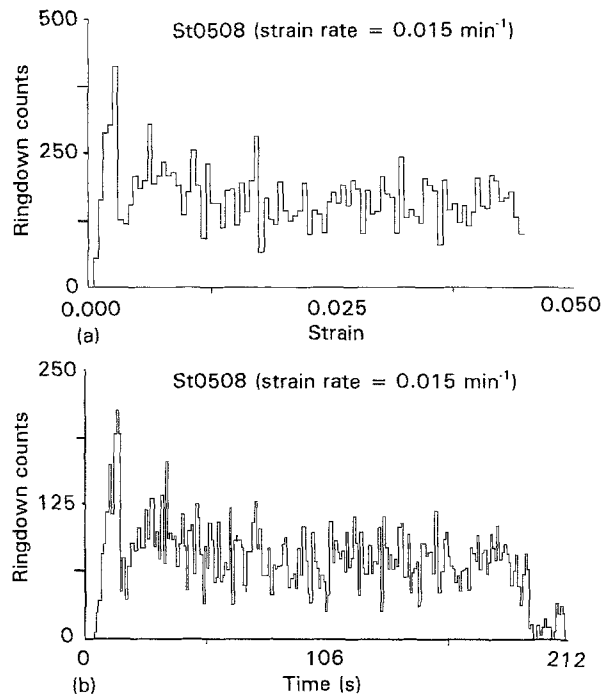Figure 9 Strain-dependence of AE counting in strain-controlled test. (a) Counts versus strain; (b) counts versus time.

expressed as

$$\dot{\varepsilon}_p = \Phi b \rho_m \bar{v} \tag{14}$$

where Φ is a geometric constant, b is Burger's vector, ρ_m is the mobile dislocation density, and $\bar{v}$ is the average velocity of dislocation motion. Fig. 11 shows the relation between strain and time during the
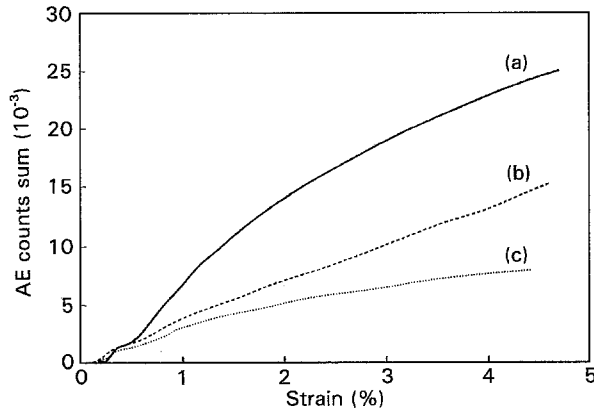
Figure 10 Strain-dependence of total ringdown counts in strain-controlled test. ——, ST0503 (strain rate = 0.005 min⁻¹); – – – –, ST0508 (strain rate = 0.015 min⁻¹); ...., ST0401 (strain rate = 0.05 min⁻¹).
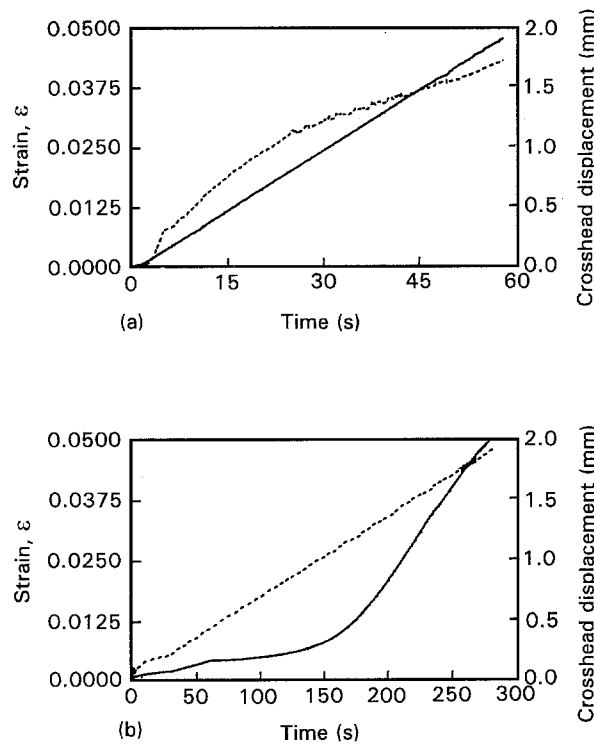

(a)

(b)

Figure 11 Strain versus time by two loading methods. (a) Strain-controlled test, constant strain rate, ——, strain versus time; (b) stroke-controlled test, constant crosshead speed, ——, strain versus time.

stress–strain test under the two loading methods. During the strain-controlled test, the strain rate was kept constant throughout the test (Fig. 11a), so that the plastic strain rate was essentially constant although the crosshead rate changed with time. Therefore, from Equation 14, ρ_m was constant because of the constant $\dot{\varepsilon}_p$ and $\bar{v}$. Thus a relation may be postulated for the strain-controlled case of the form

$$\frac{d\eta_t}{d\varepsilon} = C_1\rho_m \tag{15}$$

$$\eta_t = C_2\rho_m(\varepsilon - \varepsilon_0) \tag{16}$$

where C_1 and C_2 are empirical constants.

During the stroke-controlled test, crosshead rate was kept constant and the strain rate changed with time (Fig. 11b). In the elastic region strain rate was constant. When macroplastic deformation began, $\dot{\varepsilon}_p$ increased until it again became essentially constant in the work-hardening region. According to Equation 14, the increasing $\dot{\varepsilon}_p$ during the yield region resulted in both ρ_m and $\bar{v}$ increasing in coordination with the significant dislocation dynamics. At this time, both multiplication and slip propagation (dislocation motion) increased with increasing $\dot{\varepsilon}_p$ until the maximum point, at which $\dot{\varepsilon}_p$ became constant. Thereafter, ρ_m become constant in Equation 14, that is $d\rho_m/d\varepsilon \approx 0$, due to the dislocation saturation observed in the decline of AE activity. From this point of view the relations of $d\eta_t/d\varepsilon$ and η_t to ρ_m in strain-controlled tests could be of the form

$$\eta_t = \begin{cases} F_y[\rho_m, H(\varepsilon)] & (\varepsilon_0 \leq \varepsilon < \varepsilon_s) \\ F_w(\rho_m, \varepsilon) & (\varepsilon \geq \varepsilon_s) \end{cases} \tag{17}$$

$$\frac{\eta_t}{d\varepsilon} = \begin{cases} C_3 f(\rho_m, \varepsilon) & (\varepsilon_0 \leq \varepsilon < \varepsilon_s) \\ C_4\rho_m & (\varepsilon \geq \varepsilon_s) \end{cases} \tag{18}$$

Note that Equations 17 and 18 are compatible with the AE activity model discussed in section 3.2. Therefore, we may conclude that the mobile dislocation density and plastic strain rate are basic parameters dominating the dislocation saturation process and AE output during a monotonic tensile test under both loading methods.

4. Discussion

The dependence of acoustic emission on dislocation motion and saturation, twinning, and decohesion and fracture of inclusions and γ' particles will be discussed in this section.

4.1. Acoustic emission due to dislocation motion

In general AE generated by dislocation motion that occurs primarily near the yield point is related to plastic strain. However, it was well-known that even in the elastic region, dislocations have been activated, since local stress concentration on the grain boundaries and other obstacles cause microyielding. Figs 5 and 6 show that AE output started when strain reached ε_0 of about 0.003 µm in the elastic region. In this case, AE activation is related to the motion of the unpinned dislocations and dislocations which break away from the weakest pins, and to the generation of dislocations by activation of sources located at the grain boundary. Activation of these sources results in a sudden localized stress relaxation of a magnitude much larger than the stress relaxation caused by a single dislocation. Part of the output of these AE sources can be recorded when the threshold is set at a suitable level. The occurrence of AE activity in the elastic range means that the processes associated with AE generation must also contribute to plastic micro-strain below yield. In addition, the mobile dislocation density ρ_m and the effective stress acting on the slip

plane increase with increasing external stress in the upper elastic region.

As macroplastic deformation begins, several mechanisms contribute to AE activity in coordination: (a) more dislocations break away from pins, which can cause the unpinning of additional nearby dislocations and result in avalanches of dislocation motion; (b) Frank–Read or grain boundary sources are significantly activated; (c) AE peak detected in the yield region is attributed to slip (slip band formation and propagation). Both dislocation multiplication and dislocation motion on the slip planes contribute to the acoustic emission.

After yielding, the material enters the work-hardening region. Typically, in a constant-crosshead-rate tensile test, AE generally drops to low level in the work-hardening region due to saturation of the dislocation dynamics, which may result from the following: (i) All the grains undergo extensive slip due to dislocation activation on several slip systems, and each grain has a very high dislocation density so that a large number of dislocation pile-ups occur around the grain boundaries. Also, slip is finely dispersed in each grain with various slip systems. Thus, dislocation multiplication due to the activation of Frank–Read or grain boundary sources as well as the breakaway of the pinned dislocations becomes more and more difficult until finally it is arrested almost entirely at large strain. (ii) Dislocation movement becomes more and more difficult and the glide distance in slip planes become very short, because of the large amount of dislocation interaction, jog formation and dislocation pile-up formation at barriers. On the other hand, because the motion of the mobile dislocations depends on whether they are edge, screw or mixed dislocations, a stress gradient is needed to cause movement. However, the stress gradient during work-hardening is much smaller than in the region before and during yield, and gradually reduces to a minimum. Thus dislocation motion becomes weaker and weaker.

In short, the dislocation dynamics during tensile deformation is a saturation process by which dislocation motion initiates in the elastic strain region, reaches a maximum just beyond yield, and finally tends towards saturation. The saturation process is reflected by AE results recorded in constant-crosshead-speed tensile tests.

4.2. Acoustic emission due to fracture of inclusions and γ' particles

Inclusions and secondary-phase particles have been recognized for many years as potential sources of acoustic emission during tensile deformation [1–2, 6–9]. Processes which may be related to AE response are inclusion decohesion and fracture, and localized yielding of the matrix induced by stress–concentration effects due to inclusion orientation. Figs 3 and 4 show typical decohesion and fracture of inclusions and γ' particles within grains and along grain boundaries. Because the elastic and plastic properties as well as thermal expansion coefficients of inclusions are generally quite different from the matrix, substan-

tial stress concentrations are built up within and near inclusions during plastic deformation. If the stresses become high enough, fracture of inclusions and microcrack growth (decohesion) along the inclusion–matrix interface will occur. Both of these processes are believed to be relatively high-speed, brittle microcrack-propagation events, and therefore are expected to be a good source of acoustic emission with large burst amplitude. On the basis of the triaxial stress field of a brittle spherical inclusion, the inclusion elastic energy (U) and the inclusion fracture stress (σ_{kk}) were derived from the Griffith brittle fracture theory [14, 17] in the form

$$U = -\frac{3}{2} S_{ij} S_{ij} \pi R^3 \frac{1 - v_u^2}{E_v} \qquad (19)$$

$$\sigma_{kk} = C \frac{E_v}{(1 - v_v^2)R} \exp\left[1.5 \frac{\sigma_m^\infty}{\sigma_0}\right] \qquad (20)$$

where deviatoric stresses (S_{ij}) correspond to a strain rate $\dot{\varepsilon}_{ij}$ and yield stress σ_0. In Equations 19 and 20 E_v and v_v are the elastic modulus and Poisson's ratio of the inclusion respectively, and R is the radius of the inclusion. C is a parameter which can be obtained from the results of a tension test, and σ_m^∞ is the remote mean normal stress which depends on the remote stress field state. According to Equation 19, the larger an inclusion, the larger is the strain energy released from the inclusion fracture, causing a higher AE burst. From Equation 20 it is seen that the larger the inclusion, the more likely is inclusion fracture to occur, because of the lower fracture stress. In other words, the size of fracturing inclusions or γ' particles that fracture decreases with increasing stress and strain.

The presence of second phase (Ni$_3$Ti-type) γ' particles led to an increase in AE activity. The mechanism of decohesion and fracture of the larger γ' particles is similar to that of inclusions. However, there exists an additional influence of γ' precipitates on acoustic emission during tensile deformation in Incoloy 901. AE signals are also generated during the particle shearing process in which large numbers of dislocations are generated and pile up at the particles. With increasing load, these dislocations ultimately move by particle shear. It is known [24] that a major strengthening effect can be attributed to the irreversible energy change occurring due to interactions between dislocations and particles as the dislocations shear through the particles. The AE output associated with the particle shearing process was also observed by the authors [14, 16, 17] during cyclic softening of Incoloy 901.

4.3. Acoustic emission due to twinning

The micrographs shown in Figs 3 and 4 and the results in Table I illustrate the deformation process of Incoloy 901, that the deformation involves twinning. Twinning is an excellent source of acoustic emission because it is frequently a catastrophic process accompanied by energy release in the form of sound [10–13]. The twinning process occurs in three stages: nucleation of a twin embryo, rapid growth of the embryo

into an observable twin, and thickening of the twin normal to its original growth direction.

Twinning and slip are two different mechanisms by which metals deform plastically. In general, twin layers hinder propagation of slip. This is clear from examination of the microstructure of deformed Incoloy 901 specimens. Figs 3 and 4 show that the slip bands are not involved in either growth twins or deformation twins. In other words, fewer slip bands imply more twins. Since twinning is a rapid process, varying the strain rate changes the proportion of deformation accommodated by slip and twinning. Increasing strain rate usually increases the amount of deformation twinning and relatively less slip will occur as strain increases. Thus, in this study, higher strain rates also resulted in less AE output due to less slip (Figs 5, 6 and 10). Nevertheless determination of acoustic emission arising only from twinning is difficult, since twinning is always accompanied by slip during Incoloy 901 deformation. Separation of the contribution due to deformation twinning to the measured acoustic emission from that of slip is at present nearly impossible.

5. Conclusions
In this paper a number of observations have been made on the acoustic emission (AE) response during deformation–damage mechanisms during tensile tests of a common aircraft engine material, Incoloy 901 superalloy. Conclusions are summarized below:

1. The results clearly show that dislocation motion, twinning and inclusion fracture cooperated to generate acoustic emission during tensile deformation of Incoloy 901. However, separation of contributions to the measured acoustic emission from each of the various sources is at present practically impossible.

2. Based on AE recorded results and microstructural examination, a model based on the dislocation–saturation process was developed to describe AE activity during elastic and plastic deformation, and to distinguish between the AE response in the yield region and in the work-hardening region.

3. The effect of strain rate on AE output was examined. The fact that the influence of strain rate on the count rate $d\eta/dt$ was positive while it was negative on the counts per strain $d\eta/d\varepsilon$ and the total count η, illustrates that the AE response during deformation is a time-dependent process.

4. The effect of loading methods on AE outputs was also examined by strain-controlled tests (constant strain rate) and stroke-controlled tests (constant crosshead speed). The difference between AE output obtained by the two loading methods confirmed that the plastic strain rate controls the deformation mechanism.

References

1. C. R. HEIPLE and S. H. CARPENTER, Acoustic emission from dislocation motion, in Acoustic Emission, edited by J. R. Matthews (Gordon and Breach Publishers, New York, 1983) p. 33.
2. H. N. G. WADLEY, C. B. SCRUBY and J. H. SPEAK, *Inter. Metals Rev.* **2**, Review 249 (1980) p. 41.
3. W. SCHAARWÄCHTER and H. EBENER, *Acta Metall.* **38** (1983) 195.
4. C. R. HEIPLE and S. M. CARPENTER, *J. Acoustic Emission* **6** (1987) 177.
5. P. P. GILIS and M. A. HAMSTAD, *Mater. Sci. Eng.* **14** (1974) 103.
6. C. R. HEIPLE and S. S. CRISTIANSEN, *J. Acoustic Emission* **5** (1986) 85.
7. C. R. HEIPLE and S. M. CARPENTER, *J. Acoustic Emission* **6** (1987) 215.
8. S. L. VAN DOREN, R. B. POND and R.E. GREEN, Jr., *J. Appl. Phys.* **47** (1976) 4343.
9. M. N. BASSIM and M. VEILLETTE, *Mater. Sci. Eng.* **50** (1981) 285.
10. L. R. F. ROSE, *J. Nondestructive Evaluation* **1** (1980) 149.
11. H. B. TEOH and K. ONO, *J. Acoustic Emission* **6** (1987) 1.
12. S. L. MCBRIDE, J. W. MACLACHLAN and B. P. PARADIS. *J. Nondestructive Evaluation* **2** (1981) 35.
13. S. H. CARPENTER and F. P. HIGGINS, *Metall. Trans. A.* **8A** (1989) 1629.
14. D. FANG, "Micro- and Macro-Evaluation of Fatigue Damage Accumulation", DSc. dissertation, Technion – Israel Institute of Technology, Haifa, Israel (1993).
15. A. FANG and A. BERKOVITS, ASME *J. Mater. Tech.*, in press.
16. D. FANG and A. BERKOVITS, *J. Acoustic Emission* **11**(2), (1993) 85.
17. D. FANG and A. BERKOVITS, "Fatigue damage mechanisms on the basis of acoustic emission measurements", in Symposium on Novel Experimental Techniques in Fracture Mechanics, ASME Winter Annual Meeting, New Orleans, USA, November (1993).
18. J. P. HIRTH and J. LOTHE, "Theory of dislocation" (McGraw-Hill Book Co., New York, 1968).
19. R. W. K. HONEYCOMBE, "The plastic deformation of metals" (St. Martin's Press, New York, 1986).
20. ASTM Standards, Annual Book of ASTM Standards, ASTM, Philadelphia, Vol.03.01 (1992) p. 609.
21. M. A. HAMSTAD and A. K. MUKHERJEE, "The dependence of acoustic emission on strain rate in 7075-T6 aluminum", Experimental Mechanics, January (1975) p. 33.
22. M. A. FRIESEL and S. H. CARPENTER, *Mater. Sci. Eng.* **68** (1984) 107.
23. H. HATANO, *J. Appl. Phys.* **47** (1976) 3873.
24. R. B. NICHOLSON, "Strengthening Methods in Crystals" (Applied Science Publishers, London, 1971).